Research Square

Preprints are preliminary reports that have not undergone peer review.
They should not be considered conclusive, used to inform clinical practice,
or referenced by the media as validated information.

Force-Position Precision Control of a Rigid- Flexible Coupling Grinding End Effector Based on Sliding Mode ADRC

Zhipeng Yu

State Key Laboratory of Precision Electronic Manufacturing Technology and Equipment, Guangdong University of Technology

Zhijun Yang

yangzj@gdut.edu.cn

State Key Laboratory of Precision Electronic Manufacturing Technology and Equipment, Guangdong University of Technology

Article

Keywords: force-position control, rigid-flexible coupling, sliding mode ADRC, grinding

Posted Date: April 2nd, 2026

DOI: https://doi.org/10.21203/rs.3.rs-9205687/v1

License: This work is licensed under a Creative Commons Attribution 4.0 International License.
Read Full License

Additional Declarations: No competing interests reported.

Date of publication xxxx 00, 0000, date of current version xxxx 00, 0000.

Force-Position Precision Control of a Rigid-Flexible Coupling Grinding End Effector Based on Sliding Mode ADRC

ZHIPENG YU[1,2], ZHIJUN YANG[1,*]

[1] State Key Laboratory of Precision Electronic Manufacturing Technology and Equipment, Guangdong University of Technology, Guangzhou 510006, China; faithfulyu@126.com(ZP.Y); yangzj@gdut.edu.cn(ZJ.Y)

[2]School of Intelligent Manufacture, ShunDe Polytechnic University, FoShan, 528300, Guangdong, China; faithfulyu@126.com(ZP.Y);

*Correspondence: yangzj@gdut.edu.cn

ABSTRACT In industrial high precise grinding process for complicated workpiece surface, traditional robotic systems based on rigid-body assumptions ignore arm elastic vibrations, lacking effective flexible control. Nonlinearities, parameter deviations and elastic deformations cause 0.1mm errors, failing precision demands. This paper proposes a rigid-flexible coupling grinding system with sliding mode ADRC(SMC-ADRC). The macro-micro structure uses flexure hinges to overcome friction and filter disturbances, with a servo-driven lead-screw for large strokes, which realizes large stroke, high precision and high response speed. SMC-ADRC integrates sliding surfaces into ADRC, with TD, LESO and sliding mode control for robustness. Simulations show SMC-ADRC outperforms APID and ADRC, with 0.08s settling time under disturbances. Experiments on aluminum and marble achieve 0.5N force accuracy(35-65N), 800μm displacement precision, <50ms convergence, and Ra=0.21μm roughness. The force-position mechanical and electrical control integration precision scheme meets high-precision grinding needs.

INDEX TERMS force-position control, rigid-flexible coupling, sliding mode ADRC, grinding

I. INTRODUCTION

In the manufacturing processes of sanitary ware, furniture, hardware, and other products, grinding[1] is a critical yet challenging process. Force control in robotics[2] also constitutes a major component of motion control. Coexisting robots involve human-robot interaction, where flexible control varies significantly across different operational targets. Existing robotic operating systems primarily rely on motion interpolation control based on rigid-body assumptions[3], neglecting elastic vibrations in robotic arms and lacking effective flexible control modules for constant-force grinding/polishing and human-robot interaction. Robots are typical nonlinear time-varying systems[4]. While control techniques[5] can compensate for nonlinearities, model parameter deviations, joint reducer backlash, contact nonlinearities, and elastic deformations in robotic arms degrade control accuracy. The comprehensive end-effector error of 6-DOF serial mechanisms typically reaches 0.1mm, failing to meet increasingly precise operational demands.

Researchers have extensively studied industrial robots for automated grinding and methods to improve grinding efficiency and quality. Many studies indicate that the flexibility of manual grinding is key to achieving optimal results. To replicate this flexibility in robotic grinding, constant-force control is essential. Scholars have enhanced flexibility by integrating macro-micro or rigid-flexible coupling mechanisms between industrial robot flanges and grinding wheels. In Ma's work[6], a 3-legged Prismatic-Prismatic-Spherical(3PPS) parallel manipulator is proposed for the development of a dexterous 3DOF force-controlled end-effector module. Literature [7] presented a passive wrist system to adapt the shape of the machining curved surface by changing its posture along with the surface. Li et al.[8] proposed a novel contact force plan and control method of robotic grinding by taking the accurate material removal at different position of the workpiece as a direct target. The contact force is planned in order to guarantee material removal requirement at different point of the workpiece. In order to track the planned force with the two degrees of freedom (DOF) smart end-effector, a 2-DOF force-position hybrid control algorithm is proposed. YU et al.[9] developed a robotic polishing system with a new active end-effector. Validation experiments are conducted with the designed robotic polishing system on a complex PMMA part. Liu et al.[10] presented the design and optimization of a variable stiffness mechanism with constant output forces. However, these mechanisms not only increase system complexity but also rely primarily on rigid component designs, which generate high-frequency

vibrations during the grinding process a characteristic particularly unfavorable for control system design.

High-precision motion platforms are widely used in the field of precision processing. The macro-micro composite motion platform is widely used in the design of the above-mentioned large-stroke high-precision motion platform. In a typical macro-micro compound motion platform, the flexible hinge can effectively solve the friction dead zone problem and has the advantage of significantly improving positioning accuracy. Therefore, the micro-motion platform often adopts the design scheme based on the flexible hinge. In literature [11], a rigid-flexible coupling motion stage is invented, which uses the elastic deformation of flexure hinges to compensate the friction dead zone. Furthermore, the high-frequency disturbance of the friction is transformed into the low-frequency elastic deformation. The PID control and the ADRC designed with eight different extended state observers (ESO) are rigorously compared.

The efficacy of grinding systems is profoundly influenced by advanced control algorithms. Scholars have conducted multidimensional investigations into algorithms achieving precision, speed, and compliance, with enhanced PID variants being prominently adopted. Lubna Farhi et al.[12] proposed a PID learning controller for rigid robotic disk grinding mechanism. The grinding forces errors, end-effector path tracking error, external interferences can be mitigated via efficient feedback. In order to improve the force tracking accuracies of the developed compliant end-effector, Chen et al.[13] designed a PI controller with first-order differential force feedforward control. Dong et al.[14] presented excellent effectiveness and stabilization for pneumatic polishing force control. The PID controller with moving average filter applied in the system can eliminate the influence of external factors and reduce the phenomenon of the force descending during the polishing tool moving. Cheng et al.[15] designed and developed a position-force decoupled polishing system based on a pneumatic force servo. The PID controller is implemented and experimentally tested in the polishing system. The effective application of PID control in sophisticated grinding operations necessitates dynamic parameter tuning contingent upon workpiece stiffness characteristics, surface geometric accuracy, and evolving process specifications.

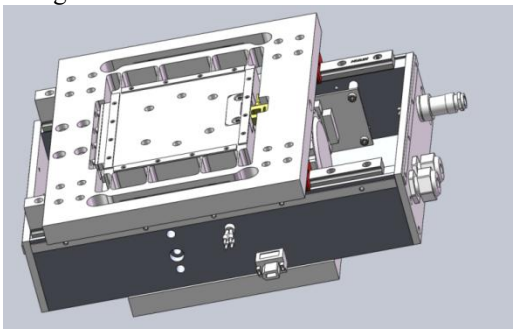
Conventional robotic design paradigms, grounded in multi-rigid-body models, inherently joint/link elasticity cannot be neglected. Practical implementations reveal that high-speed operation-induced joint clearance and elastic deformation superposition generates at least 0.1 mm systemic errors. Our methodology confronts these flexibility-induced end-effector deviations through novel flexible joint parameter identification and hybrid compensation combining rigid-flexible dynamics modeling with online parameter identification. Active Disturbance Rejection Controller (ADRC) has the advantages of fast response speed, small overshoot, high steady-state accuracy, and wide speed regulation range[16], [17], [18], [19], and it has strong robustness against system disturbances. Aiming at the problem that the normal force is easy to overshoot in the impact stage, Xiao et al.[20] used the active disturbance rejection control to plan the grinding force, and the reference force of the robot under ideal state is designed, and the speed of the robot is adjusted according to the error of actual contact force and reference force. To address time delay problem in the aero-engine blade grinding system, Shen[21] combines the improved Smith prediction algorithm with active disturbance rejection control (ADRC) to propose the filter Smith-ADRC control algorithm, which has good control effect and stability. Pazderski[22] combines the ADRC algorithm with the gradient adaptation law to online identify the unknown parameters of the plant. Parameter Identifying Disturbance Rejection Control (PIDRC) algorithm that uses the PIESO to adaptively estimate the state of the plant. Peng et al.[18] proposes a ball screw driven rigid-flexible coupling (RFC) stage to compensate for the friction dead zone by the flexure hinges. The frequency domain analysis shows that the friction is converted into elastic deformation of the flexure hinges. In addition, an active disturbance rejection control (ADRC) is designed to cancel the flexure hinges vibration and maximize the RFC stage performance. ADRC is a model-independent control algorithm renowned for its exceptional disturbance rejection capabilities. However, there remains a notable research gap: no existing literature has yet explored the application of ADRC algorithms to rigid-flexible coupling actuators in complex grinding scenarios.

This paper proposes a rigid-flexible coupled force-position hybrid grinding system based on mechanical structure design and sliding mode ADRC[23]. The system incorporates force sensors into the grinding device to enable real-time grinding force detection and adaptive stroke adjustment, achieving constant-force control during operation. On the other hand, by introducing sliding surfaces into the ADRC framework(SMC-ADRC), the system demonstrates excellent robustness against environmental disturbances, rapidly converging to sliding surfaces and maintaining stable operation along them to equilibrium points, thereby realizing fast and precise force-displacement control. Thirdly, through simulation experiments, the system's robustness was verified under various input signals and disturbance conditions. Comparative experiments with conventional Adaptive PID, ADRC and SMC-ADRC on constant-force grinding devices were conducted to evaluate response speed, grinding efficiency, and surface quality. The results demonstrate that the proposed system achieves constant-force control within 35-65N range with 0.5N accuracy, 800μm displacement precision, convergence time below 50ms, and surface roughness of Ra=0.21μm.

In this paper, section 1 provides a comprehensive literature review on complex curved surface grinding technologies, analyzing existing methodologies and identifying key challenges in the field. Section 2 details the mechanical design of the proposed rigid-flexible coupled force-position hybrid grinding system, focusing on its structural innovations and operational principles. Section 3 presents the system modeling approach and introduces a sliding-mode linear ADRC algorithm. This control strategy leverages the rapid and precise response characteristics of the rigid-flexible coupling mechanism to achieve accurate force-position control under complex disturbances. Section 4 evaluates the grinding system through simulation experiments, assessing its robustness, response time, and control precision under various operational conditions. Section 5 conducts field tests on complex workpieces, comparing the grinding efficiency and surface quality between conventional pneumatic grinding heads and the proposed system. Section 6 summarizes the key findings and contributions of this work, while outlining potential directions for future research in precision grinding technology.

II. STRUCTURAL DESIGN OF THE RIGID-FLEXIBLE HYBRID FORCE/POSITION GRINDING SYSTEM

The rigid-flexible force/position integrated grinding device employs a base frame as its structural foundation. A servo motor is mounted on the base, whose rotational motion drives a leadscrew. A leadscrew nut, installed on the leadscrew, converts the rotary motion into linear displacement. A sleeve adapter block is attached to the leadscrew nut, supporting a flexible work platform. Consequently, the reciprocating rotation of the servo motor enables precise linear motion of the flexible work platform. The flexible work platform features mounting holes, allowing the grinding head to be securely installed. A transition plate is fixed to the bottom of the base frame. Through its mounting holes, the entire rigid-flexible force-controlled grinding device can be mounted onto a fixture for operational stability. The design of the end effector is shown in fig.1.



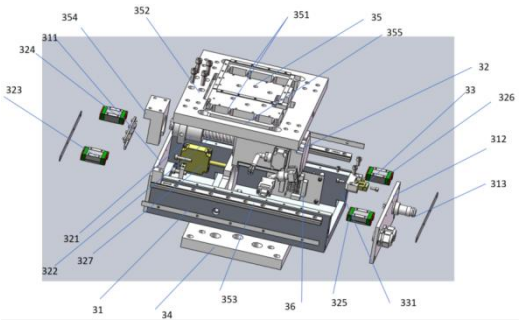


FIGURE 1. Design of the Rigid-Flexible Hybrid Force/Position Grinding End Effector.

The flexible work platform of the rigid-flexible hybrid force/position grinding device is connected to the motion platform through flexure hinges, while linear guides mounted on the base enable large-stroke linear motion of the motion platform, thereby achieving macro-positioning of the device. However, during micro motion operations, friction exists between the leadscrew and sleeve as well as between the sliding rails and rigid platform, and this friction is difficult to model precisely. The elastic deformation of flexure hinges can overcome this micro-motion friction, enabling precise motion control of the device. Moreover, the elastic deformation of flexure hinges can filter high-frequency external disturbances, thereby simplifying the frequency-domain control challenges of the system.

The gravity sensor is fixed on one side of the flexible work platform through a connection block. When the grinding head processes the workpiece, the contact grinding force is measured by the force sensor, which consists of a variable resistor (with a linear relationship between force and resistance value) and three other fixed resistors forming a bridge circuit, also known as a strain gauge. The control board reads the pressure value through A/D conversion and transmits it to the host computer via RS485 bus. Simultaneously, the servo motor control module transmits position data to the host computer through another channel of RS485 bus. Therefore, this system can achieve real-time precise control of both grinding force and displacement during the grinding process.

III. SLIDING MODE ADRC FOR FORCE-POSITION CONTROL

A servo motor-driven rigid-flexible coupled linear motion grinding end effector is mounted on the 6th axis flange of the industrial robot. This mechanism adopts a macro-micro combined rigid-flexible coupling structure, where the servo motor drives the flexible work platform through a lead screw, and the flexible work platform uses six micro-deformation plates to drive the rigid work platform sliding on the guide rails.

A pneumatic rotary grinding wheel is installed on the flexible platform of the rigid-flexible coupled linear motion grinding end effector. When the industrial robot executes the grinding trajectory, the pneumatic rotary grinding wheel rotates at high

speed to grind the workpiece surface. A force sensor is installed between the flexible platform and rigid platform to detect the contact force between the rigid-flexible coupled linear motion grinding end effector and the workpiece during grinding. The constant force control range of the rigid-flexible coupled linear motion grinding end effector can be set to any value between 5N-50N. After setting the target grinding force in the controller of the rigid-flexible coupled linear motion grinding end effector, the end effector can compare the real-time detected force from the sensor with the set grinding force to control the feed of the servo motor. During the grinding process of the industrial robot, this enables the implementation of constant force-disposition composite control on the machined surface.

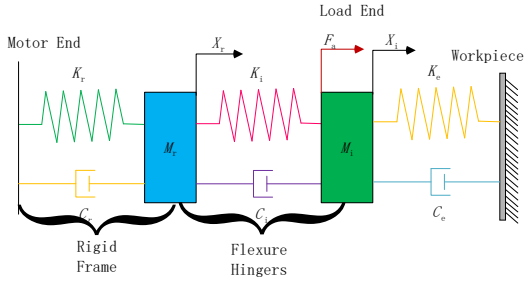


FIGURE 2. Dynamic modeling of the robot and end effector.

Within a constrained environment, ensuring the maintenance of appropriate interaction forces with the workpiece while executing compliant motion. A position-based dynamic equation is developed in this study to achieve dynamic tracking control of the desired contact force by regulating the robot's grinding and polishing forces. The model incorporates essential parameters, including stiffness, damping, and inertial components. The dynamic interaction between the controlled manipulator and the environment is effectively represented by a mass-damping-spring system. As a result, the contact model between the rigid-flexible robotic system and the environment is characterized as a second-order spring system, as depicted in Fig.2.

According to fig.2, the dynamic model of the industrial robot and the rigid-flexible coupled linear motion grinding end effector can be expressed by equation (1) :

$$M_d(\ddot{X}_d-\ddot{X}_r)+B_d(\dot{X}_d-\dot{X}_r)+K_d(X_d-X_r)=-(F_e-F_r) \quad (1)$$

where M_d、B_d and K_d represent the mass coefficient matrix, damping coefficient matrix, and stiffness coefficient matrix of the rigid-flexible coupled linear motion grinding end effector, respectively. X_d and X_r denote the actual environmental position matrix and desired environmental position matrix, while F_e and $F_r$correspond to the actual contact force matrix and desired contact force matrix when the end effector interacts with the environment.

After Lyapunov transformation, the transfer function can be expressed as (2):

$$\Delta E(s) = \frac{-\Delta F(s)}{M_d s^2+B_d s+K_d} \quad (2)$$

where $\Delta E(s) = X(s) - X_r(s), \Delta F(s) = F_e(s) - F_r(s)$.

A. TRACKING DIFFERENTIATOR(TD)

The Tracking Differentiator (TD) serves in the front part of Active Disturbance Rejection Control (ADRC). It provides derivative estimates without direct differentiation that avoids noise amplification, and introduces deliberate phase lag to maintain causality, so TD generates smooth, noise-resistant reference signals. Moreover, TD enables acceleration feedforward through extracted higher-order derivatives so it can enhance the transient performance. Thirdly, TD allows independent tuning of response speed (via speed factor R) and noise attenuation to promote the decoupling of the control system. We need to generate a smooth estimates for reference trajectory X_r and its differential signal. A second-order TD described in (3) is designed.

$$\begin{cases} \dot{v}_1 = v_2 \\ \dot{v}_2 = -r^2(v_1 - X_r) - 2rv_2 \end{cases} \quad (3)$$

where v_1 traces X_r, v_2 is the differential estimation of X_r. The increasing of r improves tracking speed but may amplify measurement noise. The characteristic equation of (3) is $s^2 + 2rs + r^2 = 0$, whose root is $s = -r$(repeated root) assuring fast tracking without overshoot.

B. LINEAR EXTENDED STATE OBSERVER (LESO)

LESO simultaneously estimates the position, velocity states of the system. It observes the total disturbance including the internal model uncertainties and external disturbances. By treating nonlinearities and cross-couplings as part of the total disturbance and transforming the system into a cascaded integral form for simplified control design, LESO realizes dynamic linearization. Through the proper choice of observer bandwidth ω_o, LESO compensates abrupt disturbances and noises. According to (1), we estimate the total system disturbance (including unmodeled dynamics and external forces) and reformulate the original system into state-space form as (4).

$$\begin{cases} \dot{x}_1 = x_2 \\ \dot{x}_2 = x_3 + b_0 u \\ \dot{x}_3 = f(x_1, x_2, w) \end{cases} \quad (4)$$

where $x_1 = e, x_2 = \dot{e}, x_3$ is the total disturbance, $b_0 = 1/M_d$, f is disturbance dynamics. Then we design 3-order ESO as (5).

$$\begin{cases} \dot{z}_1 = z_2 + \beta_1(e - z_1) \\ \dot{z}_2 = z_3 + \beta_2(e - z_1) + b_0 u \\ \dot{z}_3 = \beta_3(e - z_1) \end{cases} \quad (5)$$

According to the bandwidth method, with the observer bandwidth set as ω_o, the gains are determined as:

$$\beta_1 = 3\omega_o, \beta_2 = 3\omega_o^2, \beta_3 = \omega_o^3 \quad (6)$$

The observer gains are designed to ensure the characteristic equation of observation error dynamics satisfies:$(s + \omega_o)^3 = 0$, thereby guaranteeing exponential convergence.

C. DESIGN OF SLIDING SURFACE

A sliding surface s is constructed to enforce system state convergence to s=0, stabilizing the error dynamics. We define displacement error $e = X_d - X_r$, velocity error $\dot{e} = \dot{X}_d - \dot{X}_r$, accelerated velocity error $\ddot{e} = \ddot{X}_d - \ddot{X}_r$. Combined with second-order dynamic characteristics of the system, the integral sliding mode surface is chosen:

$$s = \dot{e} + \lambda e \ (\lambda > 0) \tag{7}$$

λ is the slope of the sliding mode surface, which can adjust the dynamic response speed and robustness. The original dynamic equation is substituted to ë, we get:

$$M_d\ddot{e} + B_d\dot{e} + K_d e = -\Delta F \tag{8}$$

After modulation, we get:

$$\ddot{e} = -\frac{1}{M_d}(B_d\dot{e} + K_d e + \Delta F) \tag{9}$$

D. NONLINEAR STATE ERROR FEEDBACK(NLSE) AND SLIDING MODE CONTROL LAW DESIGN

The Nonlinear State Error Feedback (NLSEF) in ADRC enhances transient performance by combining nonlinear error processing with adaptive disturbance rejection. By synergizing with the LESO, NLSEF compensates residual disturbances beyond LESO's bandwidth, providing >15dB better high-frequency (>100Hz) disturbance attenuation. The nonlinear feedback structure tolerates partly parameter uncertainties and operates stably dynamic ranges. This allows microsecond-level computation suitable for high-speed applications while maintaining sub-micron tracking accuracy in precision motion systems. Combing the sliding surface design and LESO disturbance compensation, we design the robust control law. The estimation total disturbance is z_3, the controlled quantity is designed as:

$$u = u_0 - \frac{z_3}{b_0} \tag{10}$$

where u_0 is the nominal control quantity. Next we design the sliding mode control law. The nominal control quantity u_0 should drive the sliding mode ε to 0.

$$u_0 = -k_1 s - k_2 sat(s/\phi) \tag{11}$$

In (11), k_1 is linear gain that adjust the convergence speed, $-k_2$ is the switch gain that suppressed the disturbance. Φ is boundary layer thickness, $sat(s/\phi)$ is saturation function :

$$sat(s/\phi) = \begin{cases} sign(s) & |s| \geq \phi \\ s/\phi & |s| < \phi \end{cases} \tag{12}$$

It can smooth the control signal and reduce the vibration. The work flow of the whole control system is shown in fig.3.

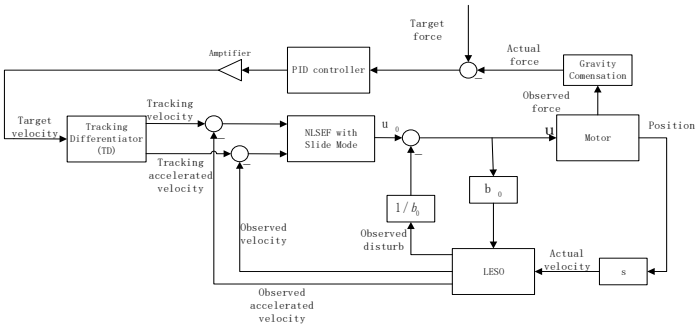


FIGURE 3. The schematic diagram of Sliding Mode ADRC.

E. CLOSED-LOOP SYSTEM STABILITY ANALYSIS

To verify the Lyapunov Stability of the Closed-Loop System, we combine the control law $u = u_0 - z_3/b_0$ with the original system dynamics, the closed-loop error equation is derived as:

$$\ddot{e} = -\frac{1}{M_d}(B_d\dot{e} + K_d e) + \frac{1}{M_d}\left(u_0 - \frac{z_3}{b_0}\right) - \frac{\Delta F}{M_d} \tag{13}$$

When LESO estimates the system disturbance precisely ($z_3 \approx \Delta F$), equation (13) can be simplified to:

$$\ddot{e} = -\frac{1}{M_d}(B_d\dot{e} + K_d e) + \frac{u_0}{M_d} \tag{14}$$

Equation (14) is substituted to sliding surface $s = \dot{e} + \lambda e$. Its derivative is:

$$\dot{s} = \ddot{e} + \lambda\dot{e} = \frac{u_0}{M_d} - \frac{B_d\dot{e} + K_d e}{M_d} + \lambda\dot{e} \tag{15}$$

We design $u_0 = -M_d(\lambda\dot{e} + \eta \cdot \mathrm{sign}(s)) + B_d\dot{e} + K_d e$ and get:

$$\dot{s} = -\eta \cdot sign(s) \tag{16}$$

The derivative of Lyapunov function satisfies:

$$\dot{V} = s\dot{s} = -\eta|s| \leq 0 \tag{17}$$

It indicates that the system will convergence onto the sliding surface $\dot{s} = 0$ in finite time, which realizes Steady-state tracking precision.

IV. SIMULATION

In this paper, we adopt the method of combining simulation analysis and experimental verification, firstly, we conduct simulation analysis in Matlab/Simulink, and then carry out experimental verification in the blade grinding system. In this way we can verify the effectiveness of the algorithm and acknowledge parameters values in theory. Simulation results show that the force overshoot of the filter SMC-ADRC control method is 0.23N, and the settling time is 0.36s. Compared with other control methods[24], [25], [26], it has good control effect, can overcome the influence of time delay problem of the grinding system, obtain good surface quality, and satisfy the requirements of the actual industry.

A. ROBUSTNESS SIMULATION

The rigid-flexible coupling SMC-ADRC strategy proposed for the actual scene of grinding and polishing is suitable for constant force tracking of various complex surfaces. The APID (Adaptive PID Control), ADRC (Adaptive Disturbance Rejection Control) [39], and SMC-ADRC (ADRC with Sliding Mode) [30] algorithms are used in MATLAB R2018a/Simulink simulation platform simulates the motion control and force control of the entire rigid-flexible coupling grinding and polishing robotic system. The simulation process is based on Intel(R) Core(TM) i9-13900H CPU and Windows operating system hardware platform. The simulation content includes the following two aspects: (1) robust simulation: the force robustness performance verification simulation of the three control algorithms under expected force mutation and disturbance influence; (2) force tracking simulation: using the three control algorithms, the position tracking simulation, the constant force tracking simulation and the variable force tracking simulation are carried out for the environment of plat surface, sloped surface, sine surface, and complex surface. The whole simulation process sets the corresponding simulation parameters based on the real physical environment of the single-degree-of-freedom force-controlled end effector. Figure 5 shows a variety of control system models designed in MATLAB/Simulink, contains APID model, ADRC model and SMC-ADRC model, where each control model includes an input model, a contact force model, and a force control model. The parameters in the simulation process are shown in Table 1.

TABLE I
PARAMETERS(SCOPE) SETTING OF APID MODEL, ADRC MODEL AND SMC-ADRC MODEL

Model	Parameters
APID	$K_p = 3\sim12, K_i = 0.01\sim0.88, K_d = 1\sim50, \mu = 0.001\sim0.1, \lambda = 0.001\sim0.01$
ADRC	$\omega_c = 70, \omega_o = 100, b_0 = 20, r = 10, h = 0.001, K_p = 6000, K_d = 200, K_f = 0$
SMC-ADRC	$\omega_c = 70, \omega_o = 100, b_0 = 20, r = 10, h = 0.001, K_p = 6000, K_d = 200, K_f = 0, k_1 = 150, k_2 = 50, \phi = 0.1$

According to the APID, ADRC and SMC-ADRC algorithms, the robustness simulation of the contact force under 3 scenarios of environmental position mutation, environmental stiffness mutation, and expected contact force mutation is carried out, and the expected contact force fd=50N is set, after normalization, the scale is transferred to 1. The simulation results are shown in Fig. 4.

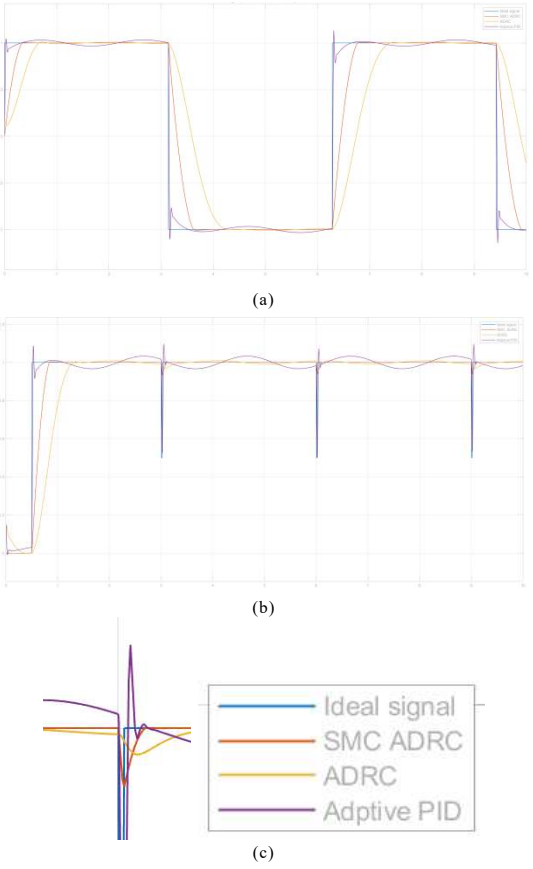


FIGURE 4. (a)Performance under a step signal, (b)Performance under external disturbances, (c) Fractionated magnifying of Fig.4.(a).

Figure 4a illustrates the performance of the three algorithms under a step signal with a period of 6.28 seconds. As shown, all three algorithms exhibit tracking capabilities for the step signal. The APID algorithm achieves the fastest tracking speed but is accompanied by significant overshoot and oscillations. In contrast, the ADRC and SMC-ADRC algorithms demonstrate minimal overshoot, accurately converging to the target value without oscillations. The ADRC algorithm requires 0.4 seconds to reach steady-state, whereas the SMC-ADRC achieves stabilization in only 0.2 seconds. Figure 4b presents the algorithms' performance under external disturbances. In this experiment, a step signal is applied, followed by periodic disturbance signals (half the amplitude of the step signal, 0.02-second pulse width) introduced every 3 seconds. The APID algorithm, which generates control signals based on output error, exhibits poor robustness. Its excessive sensitivity to disturbances results in output spikes and sustained oscillations. The ADRC algorithm shows improved disturbance rejection, albeit with a longer settling time of approximately 0.2 seconds. While the SMC-ADRC algorithm exhibits transient oscillations twice the amplitude of ADRC during disturbances (yet only 1/6 of APID's oscillations), it achieves rapid stabilization with a settling time of merely 0.08 seconds. Thus, in robustness simulation tests, the SMC-ADRC algorithm demonstrates superior performance.

B. FORCE TRACKING SIMULATION

To enhance practical effect. We simulate an uncertain part in Matlab employing the same object transfer function as described in Section 4.1. Following the methodology presented in reference[], and considering the controlled object in this project operates in a scenario characterized by micro-viscosity and strong disturbances, the initial PID parameter range for APID is set as: , we use gradient descent method to realize adaptive control. So the position error weight is set α=0.7, force error weight is set β=0.3, derivative filter time constant is set $\tau_f = 0.01$.

To implement the ADRC algorithm, the parameters of the tracking differentiator(TD) must first be determined. This project employs a discrete-time optimal tracking differentiator, which processes the input signal smoothly and extracts its differential signal. Referring to equation (3), the parameters r is set in Table.1..

For the linear extended state observer (LESO) implementation, a third-order linear ESO is adopted in this system. According to equations (4)-(5), the observer bandwidth is set as Table.1., and the gain configuration is specified in equation (6).

Furthermore, when applying the SMC-ADRC control law, the parameters of the sliding surface need to be determined. The parameter λ in equation (7) is set to 10 for the sliding surface. Combined with the disturbance compensation from LESO, the control law is designed as:

$$u = -k_1 s - k_2 sat(s/\phi) - z_3/b_0 \tag{18}$$

The values of $k_1, k_2, \phi = 0.1$ can be seen in Table.1. The simulation result is shown in fig. 5.

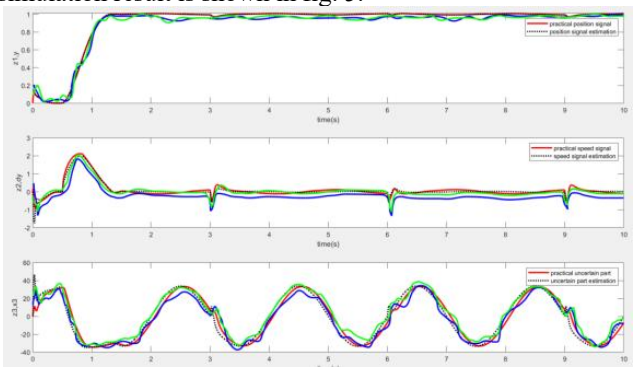


FIGURE 5. Force tracking simulation contrast.

In the simulation experiments, we emulated real-world force variations under simulation of abrasive pad wear-induced friction changes applying sudden external impacts(simulate surface irregularities) to evaluate the force tracking performance of three control algorithms.

A step force command was applied: the reference force f_d rose from 0 N to 40 N within 0.3s, stabilized at 40N for 0.3s, and then returned to 0N. Subsequently, a periodic disturbance force $f_k = -20$N was introduced every 3s. As shown in Figure 5a, all three algorithms: APID, ADRC, and SMC-ADRC achieved satisfactory steady-state tracking errors below 0.2N under stable force conditions. However, the APID algorithm exhibited the highest overshoot(5%), while ADRC and SMC-ADRC maintained overshoots within 3%. When subjected to disturbances, APID showed the longest settling time (0.2s), followed by ADRC(0.15s), with SMC-ADRC achieving the fastest convergence (0.1s).

In the other hand, a sinusoidal reference force $f_d = 40\sin(\frac{2\pi}{1.5}t)$N was applied, with a superimposed disturbance force $f_k = 5$N at specific time intervals to assess dynamic tracking capability.

As illustrated in Figure 5b, the APID algorithm demonstrated relatively inferior tracking performance, with ±5% overshoot and a prolonged settling time of 0.3 s under disturbances. The ADRC algorithm improved tracking accuracy, limiting overshoot to 3% and achieving a settling time of 0.2 s. The SMC-ADRC algorithm exhibited superior tracking precision, maintaining errors within 1% and a negligible phase lag of 0.06 s. In industrial robotic grinding applications, where typical end-effector velocities are around 50 mm/s, this phase lag is deemed acceptable. Furthermore, SMC-ADRC achieved a disturbance settling time of 0.15 s.

V. EXPERIMENT

The hardware platform of the rigid-flexible grinding robotic system is mainly composed of a PC(host computer controller), Huashu HSR-JR630 industrial robot (working range 1701mm, working load 30kg) and its control cabinet(IRC5), HANPOSE ASD240 servo motor driver (maximum power0.4KW), freud DYLY-103 force sensor (maximum force ±100N, resolution 0.1N), control board(self-development, max sampling rate 1kHz, 16bit A/D transfer resolution, 2 limit switch interfaces), RuiFen LCA326T tilt sensor(0.02° resolution, RS485 transformation), pneumatic driven grinding head(maximum torque 50Ncm, speed range 1000r–10,000r). The abrasive used is Misumi polishing disc (end face grinding and polishing) plus sandpaper (the mesh selection is 320 mesh), suitable for general curvature surface grinding and polishing. The entire rigid-flexible grinding experimental platform and communication interface are shown in Fig.6.

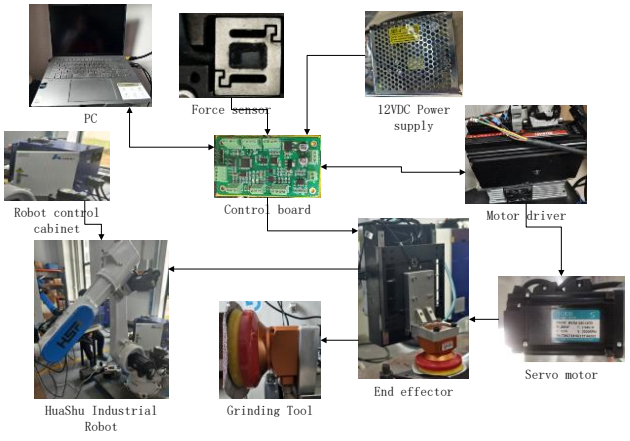


FIGURE 6. The rigid-flexible grinding robotic platform

A complete experimental cycle includes the communication time between the servo motor and the servo motor driver, the control processing time of the host computer, and the corresponding displacement time of the robot. The control bandwidth is low, and the control bandwidth of the rigid-flexible grinding robotic system is set to 1000Hz, within the normal working bandwidth of the robot for contact operation, the bandwidth of the rigid-flexible grinding robotic system in this paper meets the experimental requirements. Because the gravity of the end effector is known, we compensate the gravity through the tilt sensor while the industrial changing the pose in the process of grinding. The robot, the host computer and other devices communicate through the RS485 communication, which can ensure the reliability of the transmission rate.



FIGURE 7. Force control effect of Rigid-Flexible Coupling Grinding End Effector

According to the grinding process requirements for complex-shaped aluminum parts and marble surfaces, we conducted grinding experiments on the rigid-flexible coupling robot grinding platform. The SMC-ADRC algorithm was used in the experiments, and its parameters were set as shown in Table 1. According to the process, the grinding force needs to be set between 35 to 65N. Therefore, in the complex-shaped aluminum part target, along with the grinding path of the industrial robot (with a traveling speed of 0.1 m/s), the target grinding force was set from 35N to 65N, changing by 10N each time. The holding time for each constant force value was 5 seconds. The actual grinding force effect is shown in Figure 7. It can be seen from the figure that the target grinding force performs slightly better when rising than when falling. The oscillation time is within 0.1 seconds. Relatively speaking, when the target force is decreasing, the stabilization time is within 0.2 seconds. After the SMC-ADRC algorithm enters the steady state, the fluctuation of the target values from 35 to 55 N is within 0.5N, and the fluctuation of the 65N target value is within 1.5N. The reason should be that the industrial robot is a non-rigid body and has resonance disturbance effects during the operation of the grinding path; the pneumatic-driven grinding head is also an irregular circle and has disturbance effects during eccentric rotating. The grinding effect of the complex-shaped aluminum part is shown in Figure 8.

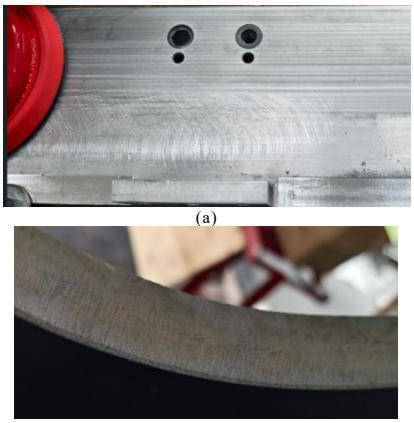


FIGURE 8. (a) Aluminum workpiece, (b) Marble face

We tested the effect of the end effector and algorithm on different workpieces with different materials: aluminum and marble workpieces. Their face was flat and curved, respectively. Because the grinding end effector has the ability to quickly control the combination of force and position, it can maintain the grinding force under the high-speed rotation of the polishing disc while the robot moves along complex trajectories. According to the process requirements, the grinding force for aluminum workpieces is 45N, while that for marble workpieces is 55N. It has been proved through experiments that the grinding surface is uniform and smooth after grinding, and the surface roughness Ra=0.21. And it presents a consistently strong polished texture. Overall, the force control effect of the rigid-flexible coupling robot grinding platform meets the requirements.

VI. CONCLUSION

The proposed rigid-flexible coupling grinding end effector, leveraging a novel Sliding Mode Active Disturbance Rejection Control (SMC-ADRC) algorithm, integrates mechanical design innovation with advanced control theory to achieve high-precision force-position regulation for complex surface grinding applications. This work bridges a critical research gap by pioneering ADRC-based control for rigid-flexible actuators in grinding scenarios, validated through Lyapunov stability analysis and high-fidelity MATLAB/Simulink simulations demonstrating >15dB superior high-frequency disturbance attenuation versus conventional Adaptive PID and ADRC. The system employs

a macro-micro architecture featuring flexure hinges to overcome friction dead zones and dampen high-frequency vibrations, coupled with a servo-driven lead-screw mechanism enabling 800μm displacement precision, while the SMC-ADRC controller innovatively combines a sliding surface with LESO to dynamically estimate and reject total disturbances, including joint elasticity, environmental uncertainties, and pneumatic grinding head eccentricities, resulting in a 50ms convergence time and 0.5N force accuracy within 35-65N operating range.In the experiment, SMC-ADRC reduced force overshoot to 3% and settling time by 50% compared to alternatives, confirming steady-state fluctuations below 1.5N under resonant disturbances, thereby offering a robust, model-independent solution for human-robot collaboration and precision manufacturing.The system enhances industrial grinding efficiency for sanitary ware, furniture, and hardware by enabling real-time adaptive stroke adjustment via force-position control , supporting complex trajectories at 0.1m/s feed rates while maintaining Ra=0.21μm surface roughness on aluminum and marble workpieces.

For the better application of the system in this article, in the future, we will focus on the embedded AI-driven parameter optimization using reinforcement learning for real-time adaptation to varying grinding processing properties. What's more, we will build standardized safety protocols for human-robot collaboration under ISO/TS 15066 during high-frequency operations.

DECLARATIONS

Ethical approval The Ethic statement is not applicable. This study does not include any animal or human studies.

Consent for publication This is to confirm that the manuscript titled "Force-Position Precision Control of a Rigid-Flexible Coupling Grinding End Effector Based on Sliding Mode ADRC"we are submitting has never been published before.Also, it is not currently being considered for publication in any other journal.All the listed authors have carefully reviewed and approved this manuscript We all agree to submit it to International Journal of Computational Intelligence Systems for publication and are aware of and accept the journal's publication policies.

Availability of data and materials The data sets presented during the current study are available from the corresponding author on reasonable request.

Competing interests The authors have no relevant financial or nonfinancial interests to disclose.

Funding This work was funded by Research and Application of Key Technologies for Robot Intelligent Operating System, Nanhai District Key Field Science and Technology Research Project, Project Number: 2230032004637

Authors' contributions First and foremost, we are profoundly grateful to our doctoral supervisor, Professor ZJ.Y, for his invaluable guidance throughout this project. His profound expertise was pivotal in shaping the mechanical design concept of the grinding end-effector and the underlying control algorithm, providing a solid foundation for this work. Author ZP.Y was the main executor of this project. He designed and verified the algorithms and made the comparisons in the experiments. He finishes the main part of the paper work.

Acknowledgements We extend our special thanks to the stuff from the State Key Laboratory of Precision Manufacturing for their insightful assistance and constructive discussions during the design and refinement of the novel algorithm. Thanks for their diligent efforts in the assembly, calibration, and debugging of the experimental setup. Their technical support was crucial in ensuring the smooth execution of the practical experiments.

Furthermore, we acknowledge Associate Dean Xing Zhou and Engineer Wanli Ouyang from the Intelligent Equipment Research Institute for generously providing access to the advanced experimental equipment and the necessary industrial-grade scenarios, which were essential for validating the system's performance under realistic conditions.

REFERENCES

[1] O. Alexa *et al.*, "A Review of Mathematical Models Used to Estimate Wheeled and Tracked Unmanned Ground Vehicle Kinematics and Dynamics," *Mathematics*, vol. 11, no. 17, p. 3735, Aug. 2023, doi: 10.3390/math11173735.

[2] X. Ke *et al.*, "Review on robot-assisted polishing: Status and future trends," *Robotics and Computer-integrated manufacturing*, vol. 80, p. 102482, 2023.

[3] J. Yang, H. Chen, R. Qi, H. Ding, and Y. Yin, "A novel approach to robotic grinding guaranteeing profile accuracy using rigid-flexible coupling force control for free-formed surfaces," *CIRP Annals*, vol. 72, no. 1, pp. 313–316, 2023, doi: 10.1016/j.cirp.2023.04.069.

[4] H. Zhou, S. Ma, G. Wang, Y. Deng, and Z. Liu, "A hybrid control strategy for grinding and polishing robot based on adaptive impedance control," *Advances in Mechanical Engineering*, vol. 13, no. 3, p. 16878140211004034, Mar. 2021, doi: 10.1177/16878140211004034.

[5] F. Xie, Z. Chong, X.-J. Liu, H. Zhao, and J. Wang, "Precise and smooth contact force control for a hybrid mobile robot used in polishing," *Robotics and Computer-Integrated Manufacturing*, vol. 83, p. 102573, Oct. 2023, doi: 10.1016/j.rcim.2023.102573.

[6] K. Ma and G. Yang, "Kinematic design of a 3-DOF force-controlled end-effector module," in *2016 IEEE 11th Conference on Industrial Electronics and Applications (ICIEA)*, Hefei, China: IEEE, Jun. 2016, pp. 1084–1089. doi: 10.1109/ICIEA.2016.7603743.

[7] L. Jiang *et al.*, "Development of a Multi-DOFs Pneumatic Servo Polishing Robot," in *2018 IEEE International Conference on Robotics and Biomimetics (ROBIO)*, Kuala Lumpur, Malaysia: IEEE, Dec. 2018, pp. 2165–2170. doi: 10.1109/ROBIO.2018.8664875.

[8] D. Li, J. Yang, H. Zhao, and H. Ding, "Contact force plan and control of robotic grinding towards ensuring contour accuracy of curved surfaces," *International Journal of Mechanical Sciences*, vol. 227, p. 107449, Aug. 2022, doi: 10.1016/j.ijmecsci.2022.107449.

[9] Y. Yu, R. Wang, Y. Wang, Y. Sun, School of Mechanical Engineering, Dalian University of Technology, Dalian

116024, China, and School of Mechanical Engineering, Dalian University of Technology, Dalian 116024, China, "Contact force controlled robotic polishing for complex PMMA parts with an active end-effector," *Journal of Advanced Manufacturing Science and Technology*, vol. 1, no. 4, pp. 2021012–0, 2021, doi: 10.51393/j.jamst.2021012.

[10] H. Liu, D. Zhu, and J. Xiao, "Conceptual design and parameter optimization of a variable stiffness mechanism for producing constant output forces," *Mechanism and Machine Theory*, vol. 154, p. 104033, Dec. 2020, doi: 10.1016/j.mechmachtheory.2020.104033.

[11] Z. Yang, R. Huang, S. Chen, L. Su, and R. Li, "Structural design and active disturbance rejection control of rigid-flexible coupling motion stage for nanopositioning," *Journal of the Franklin Institute*, vol. 360, no. 3, pp. 2133–2158, Feb. 2023, doi: 10.1016/j.jfranklin.2022.12.030.

[12] L. Farhi and F. U. Rehman, "Active Compliant PID Learning Control for Grinding Robots," *Mehran Univ. res. j. eng. technol.*, vol. 40, no. 4, pp. 747–752, Oct. 2021, doi: 10.22581/muet1982.2104.05.

[13] H. Chen, J. Yang, and H. Ding, "Robotic compliant grinding of curved parts based on a designed active force-controlled end-effector with optimized series elastic component," *Robotics and Computer-Integrated Manufacturing*, vol. 86, p. 102646, Apr. 2024, doi: 10.1016/j.rcim.2023.102646.

[14] J. Dong, J. Shi, C. Liu, and T. Yu, "Research of Pneumatic Polishing Force Control System Based on High Speed On/off with PWM Controlling," *Robotics and Computer-Integrated Manufacturing*, vol. 70, p. 102133, Aug. 2021, doi: 10.1016/j.rcim.2021.102133.

[15] F. Cheng, Z. Qizhi, Z. Lei, and Z. Hongmiao, "Development of the Polishing Tool System Based on the Pneumatic Force Servo," 2017.

[16] R. Madonski, M. Ramirez-Neria, and W. Giernacki, "Active Disturbance Rejection Control of High-Order Flat Underactuated Systems: Mass-Spring Benchmark Problem," in *Advanced, Contemporary Control*, vol. 1196, A. Bartoszewicz, J. Kabziński, and J. Kacprzyk, Eds., in Advances in Intelligent Systems and Computing, vol. 1196. , Cham: Springer International Publishing, 2020, pp. 1336–1347. doi: 10.1007/978-3-030-50936-1_111.

[17] Han Zhang, Shen Zhao, and Zhiqiang Gao, "An active disturbance rejection control solution for the two-mass-spring benchmark problem," in *2016 American Control Conference (ACC)*, Boston, MA, USA: IEEE, Jul. 2016, pp. 1566–1571. doi: 10.1109/ACC.2016.7525139.

[18] H. Peng, H. Sun, Z. Yang, W. Xue, and S. Chen, "Comparison of Several Active Disturbance Rejection Control Methods for Rigid-Flexible Coupling Motion Stage," presented at the 2019 Chinese Control Conference (CCC), Jul. 2019, pp. 3278–3283. doi: 10.23919/ChiCC.2019.8866135.

[19] H. Peng, Z. Yang, W. Xue, R. Huang, and Y. Huang, "The Design and Control of a Rigid-Flexible Coupling Positioning Stage for Enhanced Settling Performance," *Journal of Dynamic Systems, Measurement, and Control*, vol. 143, no. 11, p. 111003, Nov. 2021, doi: 10.1115/1.4051295.

[20] M. Xiao, T. Zhang, Y. Zou, and S. Chen, "Robotic constant force grinding control based on grinding model and iterative algorithm," *IR*, vol. 48, no. 2, pp. 270–279, Jul. 2021, doi: 10.1108/IR-08-2020-0166.

[21] K. Shen, S. Dai, W. Ji, and R. Wang, "Study on the constant force control of aero-engine blade grinding robot considering time delay," *Int J Adv Manuf Technol*, vol. 131, no. 3–4, pp. 1427–1447, Mar. 2024, doi: 10.1007/s00170-024-13029-5.

[22] R. Patelski and D. Pazderski, "Parameter Identifying Disturbance Rejection Control With Asymptotic Error Convergence," *IEEE Robot. Autom. Lett.*, vol. 9, no. 2, pp. 1035–1042, Feb. 2024, doi: 10.1109/lra.2023.3339942.

[23] Z. Zhang and H. Zhang, "Fractional-Order Sliding Mode with Active Disturbance Rejection Control for UAVs," *Applied Sciences*, vol. 15, no. 2, p. 556, Jan. 2025, doi: 10.3390/app15020556.

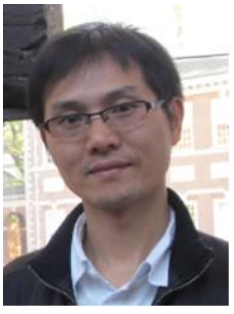
[24] S. Jiang, G. Zhao, F. Huang, W. Liu, Y. Chen, and L. Zhang, "A double closed loop digital hydraulic cylinder position system based on switching active disturbance rejection control," *Sci Rep*, vol. 15, no. 1, p. 1556, Jan. 2025, doi: 10.1038/s41598-025-85640-9.

[25] X. Bao, Y. Li, and Z. Wang, "Direct Force Control Technology for Longitudinal Trajectory of Receiver Aircraft Based on Incremental Nonlinear Dynamic Inversion and Active Disturbance Rejection Controller," *Machines*, vol. 13, no. 6, p. 525, Jun. 2025, doi: 10.3390/machines13060525.

[26] C. Jiang, Z. Yang, J. Zheng, B. Fu, and Y. Bai, "Research on Active Disturbance Rejection Control of Rigid–Flexible Coupled Constant Force Actuator," *Actuators*, vol. 14, no. 7, p. 325, Jun. 2025, doi: 10.3390/act14070325.



Zhipeng Yu, associate professor, doctoral degree. Research direction: intelligent manufacturing and robotics, precision motion and control algorithms. ORID: 0009-0000-0943-5471



Zhijun Yang, professor, doctoral student, research direction: Semiconductor packaging and testing equipment, precision operation and control technology. , ORID: 0000-0003-1927-1209

Supplementary Files

This is a list of supplementary files associated with this preprint. Click to download.

- Grindingforcedata.rar